Electron Vortices in Femtosecond Multiphoton Ionization

D. Pengel, S. Kerbstadt, D. Johannmeyer, L. Englert, T. Bayer, and M. Wollenhaupt[†]
Carl von Ossietzky Universität Oldenburg, Institut für Physik, Carl-von-Ossietzky-Straße 9-11, D-26129 Oldenburg, Germany
(Received 26 August 2016; published 2 February 2017)

Multiphoton ionization of potassium atoms with a sequence of two counter-rotating circularly polarized femtosecond laser pulses produces vortex-shaped photoelectron momentum distributions in the polarization plane describing Archimedean spirals. The pulse sequences are produced by polarization shaping and the three-dimensional photoelectron distributions are tomographically reconstructed from velocity map imaging measurements. We show that perturbative ionization leads to electron vortices with c_6 rotational symmetry. A change from c_6 to c_4 rotational symmetry of the vortices is demonstrated for nonperturbative interaction.

DOI: 10.1103/PhysRevLett.118.053003

Since the first experiment revealing the wave-particle duality of electrons [1] predicted by de Broglie [2], the interference of matter waves has been observed in numerous experiments and thoroughly studied theoretically. Nowadays, ultrashort shaped laser pulses are routinely used to manipulate matter-wave interferences, enabling control of coherent quantum dynamics (see for example, monographs [3–5]). In particular, control of the interference of free-electron wave packets has been demonstrated by photoionization with phase-locked femtosecond (fs) pulse pairs [6] or attosecond pulses [7]. Refined experimental techniques such as angular-resolved photoelectron spectroscopy provide highly differential information on the structure of those interfering electron wave packets [8]. Moreover, tomographic reconstruction of the full three-dimensional (3D) photoelectron momentum distribution [9,10] has been developed to characterize free-electron wave packets, which arise from photoionization with polarization-shaped pulses. Coherent manipulation of photoelectron angular distributions by shaped fs laser pulses has been demonstrated experimentally [11] and discussed theoretically [12]. Recently, the creation of a vortex-shaped photoelectron momentum distribution, created by photoionization with two time-delayed counter-rotating circularly polarized attosecond laser pulses, was theoretically predicted and characterized as "an unusual kind of Ramsey interference" [13].

In this Letter, we report on the experimental observation of vortex-shaped electron wave packets arising from the interference of time-delayed free-electron wave packets with different magnetic quantum numbers m. In the experiment, we detect photoelectrons with energy and angular resolution from resonance-enhanced multiphoton ionization (REMPI) of potassium atoms using a pair of time-delayed phase-locked fs pulses with counter-rotating circularity (CCP pulse pairs), generated by a polarization shaper [14–16]. Projections of the photoelectron momentum distribution are measured in a velocity map imaging (VMI) [17] setup at different angles to yield the 3D photoelectron momentum distribution by tomographic reconstruction. In the perturbative limit, electron vortices with c_6 rotational symmetry are observed, whereas nonperturbative excitation with π pulses [18] gives rise to electron vortices with c_4 rotational symmetry. The maxima of the vortices describe Archimedean spirals. The energy separation of the spiral arms is controlled by the intrapulse time delay. Pulse pairs starting with a right-handed circularly polarized pulse, followed by the second left-handed circularly polarized pulse (RLCP), create counterclockwise-rotating electron vortices, whereas clockwise-rotating electron vortices are generated by pulse pairs with the reverse ordering of polarizations (LRCP). The interplay of three distinct physical mechanisms, controlled by the polarization of the pulses, the field intensity, and the time delay τ between the two pulses, enables coherent control. Polarization control is achieved by the CCP pulse pairs: each pulse defines a single ionization pathway due to the selection rules $\Delta l = 1$ and $\Delta m = \pm 1$ for $\sigma^{\pm}$ transitions. Perturbative excitation leaves the ground-state population unchanged so that both pulses interact with the quantum system essentially in the ground state. In contrast, the population dynamics during nonperturbative interaction of the first pulse with the quantum system controls the initial conditions for the second laser pulse. The time evolution of the initially created electron wave packet results in an energy-dependent (relative) phase of $-\tau E/\hbar$, where E denotes the variable excess energy of the electron. The schemes for $1+2$ REMPI of potassium atoms using right- and left-handed circularly polarized light ($\mathcal{E}_R$ and $\mathcal{E}_L$) for perturbative and nonperturbative interactions are depicted in Fig. 1(a) and Fig. 1(b), respectively. Ionization with two right-handed circularly polarized pulses (RRCP) proceeds via the $|s,0\rangle \xrightarrow{\mathcal{E}_R} |p,-1\rangle \xrightarrow{\mathcal{E}_R} |d,-2\rangle \xrightarrow{\mathcal{E}_R} |f,-3\rangle$ states, where $|l,m\rangle$ characterizes the angular part of the wave function. When the second electron wave packet is created, the first electron wave packet has acquired a phase of $-\tau E/\hbar$ due

 © 2017 American Physical Society

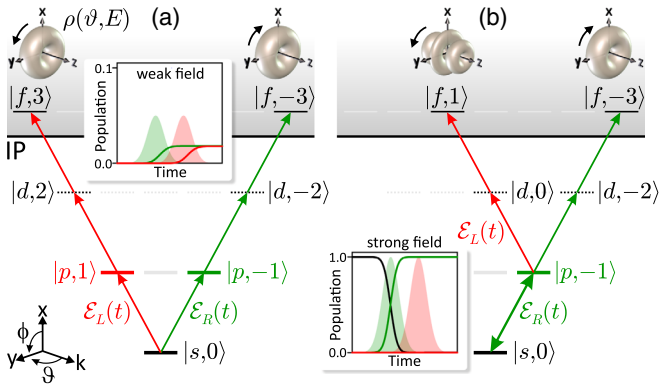

FIG. 1. Ionization scheme for $1+2$ REMPI of potassium atoms with left- and right-handed circularly polarized light ($\mathcal{E}_L$ and $\mathcal{E}_R$), including intermediate states and the interfering final electron wave packets. The insets show the population dynamics of the $|p,1\rangle$ and $|p,-1\rangle$ states (a) for perturbative interaction and (b) excitation with π pulses.

to the time delay between the two pulses. Therefore, three-photon ionization with RRCP pulse pairs produces the coherent superposition state

$$|\psi\rangle \propto e^{-i\tau E/\hbar}|f,-3\rangle + |f,-3\rangle. \tag{1}$$

With Ω representing the angular coordinates ϑ and ϕ (see Fig. 1), and $\langle\Omega, E|l,m\rangle \propto \Psi_{l,|m|}(\vartheta,E)e^{im\phi}$ the projection on Ω and E, the probability density for the superposition state reads

$$|\psi(E,\Omega)|^2 \propto [1+\cos(\tau E/\hbar)]\rho(\vartheta,E). \tag{2}$$

Herein, $\rho(\vartheta,E) = |\Psi_{3,3}(\vartheta,E)|^2$ describes the torus-type photoelectron distribution obtained for single pulse ionization [cf. Fig. 1(a)]. The experimental result for ionization with an RRCP pulse pair depicted in Fig. 4(a) shows characteristic interference fringes with an energy separation of $\Delta E_F = h/\tau$ in the radial (energy) direction. More quantum pathways are available when CCP pulse pairs are used for ionization. Ionization with an RLCP pulse pair starts with a right-handed circularly polarized pulse (RCP) and proceeds via the same pathway as above. In the perturbative limit, the $|s,0\rangle$ ground-state population remains essentially unchanged by the first pulse [cf. inset to Fig. 1(a)] and therefore, ionization with the second left-handed circularly polarized pulse (LCP) proceeds similarly via the $|s,0\rangle \xrightarrow{\mathcal{E}_L} |p,1\rangle \xrightarrow{\mathcal{E}_L} |d,2\rangle \xrightarrow{\mathcal{E}_L} |f,3\rangle$ states. Therefore, for ionization with RLCP pulses, the wave packet ends up in a coherent superposition of states with different quantum numbers $m = \pm 3$:

$$|\psi_6\rangle \propto e^{-i\tau E/\hbar}|f,-3\rangle + |f,3\rangle. \tag{3}$$

The angle-dependent interference of the two states $\langle\Omega|f,-3\rangle \propto e^{-3i\phi}$ and $\langle\Omega|f,3\rangle \propto e^{3i\phi}$ exhibits c_6 symmetry. The vortex structure arises from the additional interference in radial (energy) direction, given by the amplitude $e^{-i\tau E/\hbar}$. In order to quantitatively discuss the fringe structure of the wave packet, we calculate the probability density from Eq. (3) and obtain

$$|\psi_6(E,\Omega)|^2 \propto [1+\cos(6\phi+\tau E/\hbar)]\rho(\vartheta,E), \tag{4}$$

with maxima in the interference term at

$$E_{\max}(\phi) = (2\pi n - 6\phi)\hbar/\tau \tag{5}$$

for integer values of n and $E_{\max}(\phi) > 0$. Equation (5) highlights that the maxima in the section through the energy-calibrated photoelectron distribution in the polarization plane (x-y plane) describe Archimedean spirals (cf. Fig. 5). Nonperturbative excitation with a right-handed circularly polarized π pulse creates an $|f,-3\rangle$ free-electron wave packet and depletes the $|s,0\rangle$ ground state such that after the pulse, the population is exclusively stored in the excited $|p,-1\rangle$ state [see inset to Fig. 1(b)]. Therefore, the second pulse in an RLCP sequence ionizes the excited $|p,-1\rangle$ state via the ionization pathway $|p,-1\rangle \xrightarrow{\mathcal{E}_L} |d,0\rangle \xrightarrow{\mathcal{E}_L} |f,1\rangle$. In this case, the wave packet is composed of the contributions

$$|\psi_4\rangle \propto e^{-i\tau E/\hbar}|f,-3\rangle + |f,1\rangle. \tag{6}$$

Analogous to the above discussion, the coherent superposition of the $|f,-3\rangle$ and $|f,1\rangle$ states results in c_4 rotational symmetry. The radial interference fringes introduced by the time delay are unchanged. The results from the simple physical picture presented here are supported by simulations reported in [13] and our own nonperturbative simulations described in [12], taking into account both the population dynamics and the ionization dynamics via all pathways.

The experimental setup, schematically shown in Fig. 2, combines ultrafast polarization shaping with a tomographic reconstruction technique based on VMI to measure the 3D photoelectron momentum distribution. The choice of the time delay between the pulses is restricted by three constraints: (1) in order to observe the interference pattern, the energy separation of the interference fringes $\Delta E_F = h/\tau$ needs to be larger than the energy resolution of the VMI spectrometer ΔE_S, i.e., the VMI's spectral resolution places an upper limit on the delay $\tau < h/\Delta E_S$, (2) the two pulses with duration Δt and opposite circularity need to be fully separated—otherwise the polarization in the overlap region is linear—and (3) ΔE_F needs to be well below the width of the three-photon spectrum $\Delta E_T \approx 0.76h/\Delta t$. These constraints result in $\Delta E_S < \Delta E_F < \Delta E_T$. Both the conditions (2) and (3) place a lower limit on the delay. As soon as the two pulses are fully separated, i.e., $\tau \gg \Delta t$, a

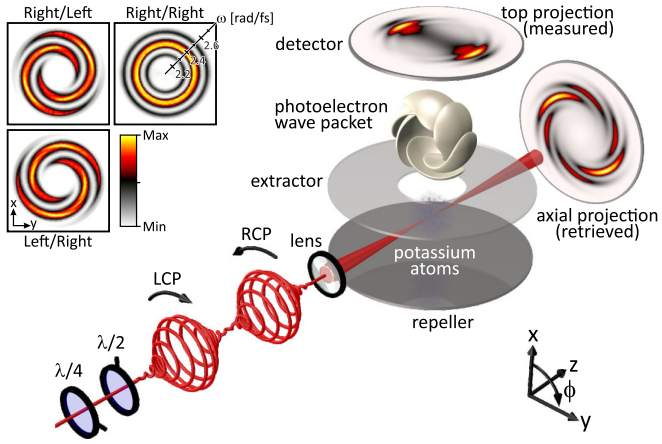

FIG. 2. Interaction of CCP pulse pairs with potassium atoms gives rise to vortex-shaped photoelectron wave packets via $1+2$ REMPI. The electron wave packets are imaged using a VMI spectrometer. A $\lambda/2$ wave plate rotates the incident CCP pulse pair for tomographic reconstruction of the 3D photoelectron momentum distribution, revealing the vortex pattern in the polarization plane (x-y plane). The insets show measured angular-resolved optical spectra of the incident pulse pairs. The color scale is identical in all figures.

sufficient number of fringes $\Delta E_T/\Delta E_F \approx 0.76\tau/\Delta t$ is visible. Taking $2\Delta t$ as the minimal delay to guarantee pulse separation, one obtains $2\Delta t \leq \tau \leq h/\Delta E_S$. Assuming $\Delta t = 20$ fs and $\Delta E_S = 80$ meV results in a narrow window 40 fs $\leq \tau \leq$ 50 fs of permissible delays.

We use a FEMTOLASERS multipass chirped-pulse amplifier (Rainbow 500, Femtopower HR 3 kHz CEP), providing p-polarized 20 fs pulses centered at 790 nm, with a full width at half maximum of 80 nm. Because the experiments are insensitive to the Carrier Envelope Phase (CEP), CEP stabilization was not used. In general, a CEP dependence is expected when multiphoton pathways of different order interfere [19] ($n\omega$ vs $m\omega$ excitation). For the generation of CCP pulses, we employ a polarization shaper in $4f$ geometry, equipped with a dual-display liquid crystal spatial light modulator (LCSLM; Jenoptik SLM-640d) [14,16,20]. The two LC displays, A and B, with optical axes tilted by $\phi_A = 45°$ and $\phi_B = -45°$, with respect to the detector axis, control the spectral phases $\varphi_A(\omega)$ and $\varphi_B(\omega)$ of the respective components of the input pulse. Shaper-based compensation of residual spectral phases is achieved by evolutionary optimization of second harmonic generation in a nonlinear crystal. Additional application of linear spectral phases $\varphi_{A,B}(\omega) = \mp(\tau/2)\omega$ delivers pairs of bandwidth-limited pulses, temporally separated by τ and orthogonally polarized along the corresponding LC axes [20]. A $\lambda/4$ wave plate, aligned either at $\phi_{\lambda/4} = 0°$ (LRCP) or at $\phi_{\lambda/4} = 90°$ (RLCP), transforms the pulse pair into a CCP pulse sequence. RRCP pulse pairs are generated by insertion of a p-aligned polarizer behind the LCSLM and the $\lambda/4$ wave plate aligned at $\phi_{\lambda/4} = 45°$. In order to verify the polarization state of the generated pulse pairs, we measured projections of the spectrum under different angles between $\phi_{\rm pol} = 0°$ and 360° using a rotatable polarizer in front of an optical spectrometer. The results are shown in the inset to Fig. 2. For RRCP pulses, the observed spectral interference fringe pattern is angle independent. For RLCP (LRCP) pulse pairs, the interference fringes rotate counterclockwise (clockwise), resulting in optical spirals with inherent c_2 symmetry. The symmetry arises due to the $\pi/2$ phase shift introduced by the $\lambda/4$ wave plate between orthogonal field components, with the opposite sign for the L- and RCP pulse. Thus, over 90°, the pulse sequence acquires an effective relative phase of π, leading to a recurrence of the interference pattern every 180°. For the detection of photoelectrons, we employed a VMI spectrometer based on our previous design [16]. The CCP pulses are focused by a lens with a focal length of 250 mm into the interaction region of the spectrometer to interact with potassium atoms provided by a dispenser source (cf. Fig. 2) at a background pressure of about 5×10^{-7} mbar. Photoelectrons released during the interaction are detected by a chevron MCP detector, followed by a phosphor screen, which is imaged onto a CCD camera. The energy calibration of the spectrometer was performed using a narrow-band laser diode tuned to the potassium $5p_{3/2}$ resonance at 404.53 nm as described in [21]. The energy resolution of the VMI was determined to be better than 80 meV at 1 eV, which allows us to resolve electron vortices for time delays of up to $\tau \approx 50$ fs. Note that the highly structured interference fringes in the images have Fourier components up to 8 times larger than those of interference-free images from single pulse ionization. In the weak-field experiments, the laser intensity was adjusted to $I_0 \approx 5 \times 10^{10}$ W cm^{-2}, resulting in about one event per laser pulse. For the nonperturbative experiment, we used an intensity of $4I_0$. In order to reveal the vortex structure of the photoelectron wave packets in the polarization plane, which is not directly measured in our setup, we retrieved the full 3D electron momentum distribution (ED). Since the electron vortices are not cylindrically symmetric (see discussion below), Abel inversion is not applicable. Instead, we employed a tomographic reconstruction technique [9–11,22], which is applicable, irrespective of the symmetry. Using a $\lambda/2$ wave plate to rotate the incident laser pulses, different projections of the electron wave packet are measured for 45 angles between −90° and 86°. From the projected electron momentum distributions (PEDs), obtained by accumulating 400 images taken with an exposure time of 200 ms each, we retrieved the ED, employing the Fourier slice algorithm [23].

We start by discussing the symmetry properties of the measured PEDs upon rotation of the ionizing pulse about its propagation direction $\boldsymbol{k}$. In general, EDs from ionization with a single circularly polarized laser pulse or an RRCP pulse pair are circularly symmetric about $\boldsymbol{k}$. This

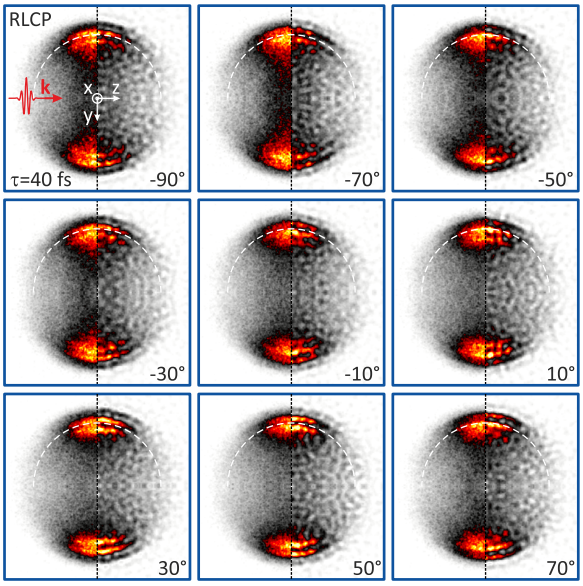

FIG. 3. Measured PEDs for different rotation angles ϕ of an RLCP pulse pair. PEDs with enhanced high frequency components, shown on the right half, emphasize the interference fringes. The dotted white lines serve as a reference to illustrate the fringe shift upon rotation.

circumstance is illustrated schematically in Fig. 1 for RCP ionization ($\mathcal{E}_R$ only) and confirmed by the experimental result for an RRCP pulse shown in Fig. 4(a). Hence, rotation of the pulse does not change the PED. However, the interference fringes in the PEDs measured at different rotation angles (between $\phi = -90°$ and 70°), depicted in Fig. 3, shift upon rotation of the ionizing CCP pulse pair although both pulses in the sequence are circularly polarized. This observation proves that the ED is not circularly symmetric. Nevertheless, measured PEDs differing from each other by rotation angles of $\Delta\phi = n \times 60°$ (displayed in the same column of Fig. 3) are very similar, i.e., $\mathrm{PED}(\phi) \approx \mathrm{PED}(\phi + n \times 60°)$. In particular, the fringe positions in those PEDs are identical. This finding already suggests an approximate c_6 symmetry of the ED. In addition, we notice that, although all measured PEDs have axial and lateral symmetry, the observed PEDs at the rotation angles $\pm\phi$ are, in general, not identical. From this observation, we conclude that the ED has no mirror plane perpendicular to the polarization plane. Next, we analyze sections through the reconstructed EDs in the polarization plane at $z = 0$, displayed in the upper row of Fig. 4. In order to enhance the visibility of the fringes in Fig. 4, the corresponding Fourier components have been scaled by a factor of 4. A vortex structure with approximate c_6 symmetry is clearly visible for both RLCP [Fig. 4(b)] and LRCP [Fig. 4(c)] pulse pairs. The maxima of the reconstructed ED section for the RLCP pulse pair shown in Fig. 4(b) rotate counterclockwise for increasing values along the energy axis. Therefore, vortices created by RLCP pulse pairs are called counterclockwise. The clockwise

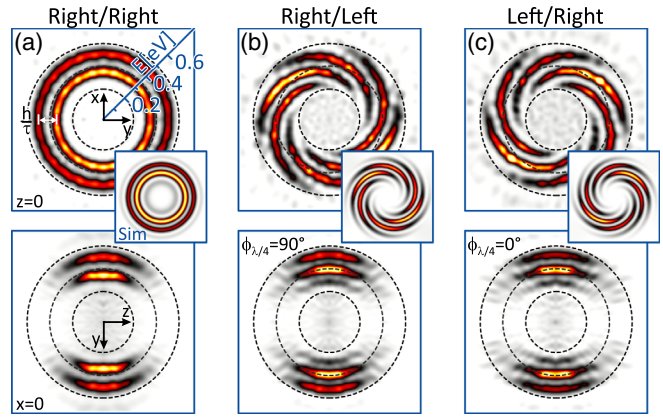

FIG. 4. Sections through the reconstructed 3D electron distribution (ED) for (a) RRCP, (b) RLCP, and (c) LRCP pulse pairs. Upper row: sections in the polarization plane at $z = 0$ compared to simulation results shown in the insets. Lower row: sections in the detector plane at $x = 0$. CCP pulse pairs generate vortex-shaped EDs in contrast to RRCP pulse pairs, which create circularly symmetric EDs.

vortex depicted in Fig. 4(c) is created by an LRCP pulse. Taking into account the handedness conventions and the orientation of the plotted sections, our experimental findings are consistent with the theoretical prediction [13]. The insets to Fig. 4 show simulated angle- and energy-resolved ED sections in the polarization plane based on the numerical solution of the time-dependent Schrödinger equation, including all relevant ionization pathways as described in [12]. Comparison to the experimental results shows excellent agreement. Both the tomographically reconstructed and the simulated ED confirm the (approximate) c_6 rotational symmetry, i.e., $\mathrm{ED}(\phi) \approx \mathrm{ED}(\phi + n \times 60°)$. A simulated vortex-shaped ED showing c_6 rotational symmetry is depicted in Fig. 2. Deviations from perfect c_6 symmetry, expressed by the inhomogeneous intensity distribution among the spiral arms in Figs. 4(b) and 4(c), are explained by minor contributions to the final state from ionization of the perturbatively excited states $|p, \pm 1\rangle$ by the second pulse [cf. Fig. 1(b)]. This analysis was confirmed by our simulations where the respective pathways could be turned off artificially. In the lower row of Fig. 4, perpendicular sections at $x = 0$, showing the reconstructed ED section in the detector plane (y-z plane), are displayed. Note that the vortices in Figs. 4(b) and 4(c) are indistinguishable when analyzed in the detection plane. By increasing the intensity of the first pulse in an LRCP sequence to a point at which the population is predominantly stored in the excited $|p, 1\rangle$ state, the ionization pathway for the second pulse changes such that the electron is guided into a superposition state analogous to Eq. (6), composed of states with different angular distributions [cf. Fig. 1(b)]. We note that the intensity was too low to observe above-threshold ionization. Figure 5(b) shows a section through the reconstructed ED in the polarization

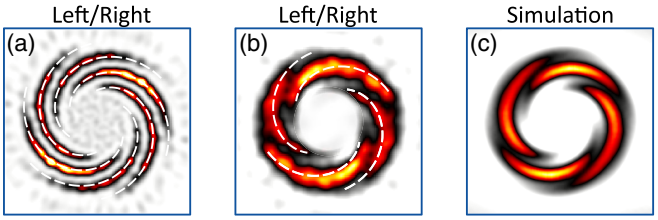

FIG. 5. Sections through the ED for (a) perturbative and (b) nonperturbative excitation with an LRCP pulse sequence show c_6 and c_4 symmetry, respectively. The reconstructed ED sections are superimposed by Archimedean spirals. The section in (b) is compared to a simulation in (c).

plane for nonperturbative ionization. Although the contours are less pronounced compared to the weak-field result due to focal intensity averaging, the approximate c_4 symmetry is clearly visible. The clearest c_4 symmetry was observed with a minimal displacement from $z = 0$, where the spiral arms appear slightly thicker. The simulated results without focal intensity averaging, shown in Fig. 5(c), are in good agreement with the reconstructed ED section in Fig. 5(b).

We have demonstrated the creation of vortex-shaped electron wave packets by perturbative and nonperturbative REMPI of potassium atoms with CCP pulse sequences generated by fs polarization shaping. Coherent control by the field polarization and intensity was shown to rely on the creation of superposition states composed of free-electron wave packets with different magnetic quantum numbers. The time delay controlled the energy-dependent amplitudes of the contributing states, causing Ramsey-type interference fringes in the radial direction. The ionization pathways were selected by the laser polarization via selection rules and the field strength via the population dynamics. The interplay of both mechanisms introduces a new twist to Ramsey-type experiments. In the experiment, tomographic reconstruction of EDs allowed us to retrieve the unusual vortex shape of the ED in the polarization plane. Although all measured PEDs exhibited both lateral and axial mirror symmetries, the reconstructed results showed c_6 rotational symmetry for perturbative interactions and c_4 rotational symmetry for strong fields. We found that RLCP (LRCP) pulse pairs generated counterclockwise- (clockwise-) rotating electron vortices describing Archimedean spirals. In the context of previous work on the determination of ionization matrix elements by polarization-shaped pulses [12,24], we believe that ionization with CCP pulse pairs is an ideal technique to measure the quantum mechanical phase of ionic states, simplified by selective excitation of only a few quantum states. Motivated by our finding that CCP pulse pairs discriminate between signatures from excitation and ionization, we currently investigate REMPI of chiral molecules with CCP pulse pairs to study the role of intermediate resonances in the multiphoton photoelectron circular dichroism [25].

Financial support by the Deutsche Forschungsgemeinschaft via the priority programme SPP1840 QUTIF is gratefully acknowledged.

†Corresponding author.
matthias.wollenhaupt@uni-oldenburg.de

[1] C. Davisson and L. H. Germer, Phys. Rev. **30**, 705 (1927).
[2] L. de Broglie, Ann. Phys. (Berlin) **3**, 22 (1925).
[3] S. A. Rice and M. Zhao, *Optical Control of Molecular Dynamics* (Wiley, New York, 2000).
[4] D. Tannor, *Introduction to Quantum Mechanics: A Time-Dependent Perspective* (University Science Books, Sausalito, California, 2007).
[5] M. Shapiro and P. Brumer, *Quantum Control of Molecular Processes*, 2nd ed. (Wiley, New York, 2011).
[6] M. Wollenhaupt, A. Assion, D. Liese, C. Sarpe-Tudoran, T. Baumert, S. Zamith, M. A. Bouchene, B. Girard, A. Flettner, U. Weichmann, and G. Gerber, Phys. Rev. Lett. **89**, 173001 (2002).
[7] F. Lindner, M. G. Schätzel, H. Walther, A. Baltuska, E. Goulielmakis, F. Krausz, D. B. Milosevic, D. Bauer, W. Becker, and G. G. Paulus, Phys. Rev. Lett. **95**, 040401 (2005).
[8] K. L. Reid, Annu. Rev. Phys. Chem. **54**, 397 (2003).
[9] M. Wollenhaupt, M. Krug, J. Köhler, T. Bayer, C. Sarpe-Tudoran, and T. Baumert, Appl. Phys. B **95**, 647 (2009).
[10] C. Smeenk, L. Arissian, A. Staude, D. M. Villeneuve, and P. B. Corkum, J. Phys. B **42**, 185402 (2009).
[11] M. Wollenhaupt, C. Lux, M. Krug, and T. Baumert, ChemPhysChem **14**, 1341 (2013).
[12] P. Hockett, M. Wollenhaupt, C. Lux, and T. Baumert, Phys. Rev. Lett. **112**, 223001 (2014).
[13] J. M. Ngoko Djiokap, S. X. Hu, L. B. Madsen, N. L. Manakov, A. V. Meremianin, and A. F. Starace, Phys. Rev. Lett. **115**, 113004 (2015).
[14] T. Brixner and G. Gerber, Opt. Lett. **26**, 557 (2001).
[15] N. Dudovich, D. Oron, and Y. Silberberg, Phys. Rev. Lett. **92**, 103003 (2004).
[16] M. Wollenhaupt, M. Krug, J. Köhler, T. Bayer, C. Sarpe-Tudoran, and T. Baumert, Appl. Phys. B **95**, 245 (2009).
[17] A. T. J. B. Eppink and D. H. Parker, Rev. Sci. Instrum. **68**, 3477 (1997).
[18] N. V. Vitanov, T. Halfmann, B. W. Shore, and K. Bergmann, Annu. Rev. Phys. Chem. **52**, 763 (2001).
[19] M. Abel, D. M. Neumark, S. R. Leone, and T. Pfeifer, Laser Photonics Rev. **5**, 352 (2011).
[20] J. Köhler, M. Wollenhaupt, T. Bayer, C. Sarpe, and T. Baumert, Opt. Express **19**, 11638 (2011).
[21] A. Wituschek, J. von Vangerow, J. Grzesiak, F. Stienkemeier, and M. Mudrich, Rev. Sci. Instrum. **87** (2016).
[22] P. Hockett, M. Staniforth, and K. L. Reid, Mol. Phys. **108**, 1045 (2010).
[23] A. C. Kak and M. Slaney, *Principles of Computerized Tomographic Imaging* (IEEE Press, New York, 1988) pp. 1–339.
[24] P. Hockett, M. Wollenhaupt, C. Lux, and T. Baumert, Phys. Rev. A **92**, 013411 (2015).
[25] C. Lux, M. Wollenhaupt, T. Bolze, Q. Liang, J. Köhler, C. Sarpe, and T. Baumert, Angew. Chem., Int. Ed. Engl. **51**, 5001 (2012).